LA-UR-07-0685

Environment Dependent Charge Potential for Water

Krishna Muralidharan
Department of Physics and Astronomy, University of New Mexico, Albuquerque, New Mexico 87131 and Quantum Theory Project, University of Florida, Gainesville, FL 32601

Steven M. Valone
Materials Science and Technology Division, Los Alamos National Laboratory, Los Alamos, New Mexico 87545 and Department of Physics and Astronomy, University of New Mexico, Albuquerque, New Mexico 87131

Susan R. Atlas*
Center for Advanced Studies and Department of Physics and Astronomy, University of New Mexico, Albuquerque, New Mexico 87131

(Dated: February 5, 2008)

We present a new interatomic potential for water captured in a charge-transfer embedded atom method (EAM) framework. The potential accounts for explicit, dynamical charge transfer in atoms as a function of the local chemical environment. As an initial test of the charge-transfer EAM approach for a molecular system, we have constructed a relatively simple version of the potential and examined its ability to model the energetics of small water clusters. The excellent agreement between our results and current experimental and higher-level quantum computational data signifies a successful first step towards developing a unified charge-transfer potential capable of accurately describing the polymorphs, dynamics, and complex thermodynamic behavior of water.

I. INTRODUCTION

Developing accurate interatomic potentials is essential for modeling the atomistic behavior of materials in diverse chemical and physical environments. Broadly speaking, potentials can be classified as empirical or semi-empirical. Empirical potentials—ranging from the relatively simple Lennard-Jones and Buckingham potentials to more elaborate force fields such as CHARMM[1] or ReaxFF[2]—are typically parameterized to represent a set of specific structural or thermodynamic properties of a given molecular system or material. Consequently they may have limited success in representing other non-parameterized properties, or materials whose atomic or molecular constituents lie outside the parametrization set. Systems where charge transfer effects are important present a particular challenge to empirical approaches. The simplest models incorporate fixed formal atomic charges with distance-dependent charge transfer switching functions.[3] Others define a charge-dependent functional form,[4] often a simple quadratic as in the ES+ method,[5] and adjust the charges via chemical potential equalization. On the other hand, semi-empirical potentials guided by quantum mechanics (QM)—for example, the embedded-atom (EAM)[7,8,9] and modified embedded-atom methods (MEAM),[10] tight-binding (TB) theory,[11] SCC-DFTB/CHARMM,[12] diatomics-in-molecules[13] and empirical valence bond (EVB) approaches[14,15]—depend on potential parameters derived from *ab initio* calculations or experimental data. The success of these semi-empirical approaches hinges upon the ability of the model to assimilate relevant QM and experimental information within a functional form that depends on a relatively small set of parameters, and can be translated readily into computer code for efficient application to large-scale simulation systems. In the case of the TB and EVB approaches, the parameterizations generally require the specification of a carefully tailored set of basis wavefunctions, the estimation of corresponding overlap integrals, and on-the-fly Hamiltonian diagonalizations. These explicit QM steps significantly complicate the construction of the potentials, thus limiting the size and chemical diversity of the systems to which they can be applied. Similarly, SCC-DFTB/CHARMM and other QM/MM methods[16] require the definition of appropriate auxiliary conditions in order to handle boundary-matching, charge polarization, and long-range electrostatic interactions between the quantum and classical (molecular mechanics) regions of the system. Semi-empirical potentials such as EAM and MEAM do not involve explicit QM components, but in their present form cannot account for non-perturbative changes in the charge states of atoms. Consequently, they are not expected to accurately model such important biophysical and materials problems as polar systems, electron transport, defect-driven charge polarization, fluctuating valence systems, complex oxides, and reactive dynamics.

In this study, we present the first implementation of a novel charge-transfer embedded atom (CT-EAM) potential aimed at addressing the issues outlined above, and apply it to the structure and energetics of netural water clusters $(H_2O)_n$, $n = 2, \ldots, 20$. Importantly, the new potential incorporates quantum mechanical information in the spirit of TB, EVB, and related approaches, while preserving the intuitive features, ease of parametrization, and extensibility of the EAM. The potential is based on a multiscale framework recently described by two of the authors.[17,18] This framework is formally based in density functional theory (DFT),[19,20] and

couples the electronic and atomistic length scales within a self-consistent classical potential. A key feature of the potential is its dependence on the redistributed atomic electron densities—and by extension, charge transfer—which vary with the instantaneous configuration of the atoms within the molecule or material. The parameterized charge distributions are derived from *ab initio* calculations. This 'atom-in-molecule' perspective and associated effective charge are at the heart of the CT-EAM model framework. A second important aspect is the imposition of self-consistency between the atomic electron densities appearing in the two physically distinct—embedding and electrostatic—components of the model. This requirement is intrinsic to the CT-EAM theory, and is in contrast to other charge transfer models, including some based on the EAM, where different functional forms are assigned to nominally identical electron densities.

For this initial implementation, we focus on water as a paradigmatic small molecule system of immense practical importance to biomolecular and materials applications. Water also represents an extremely challenging test system for any classical potential due to its strong polar features arising from underlying charge transfer and charge polarization, and associated many-body effects.[21]

In the following section we briefly review the extensive literature on classical potentials for water, with emphasis on previous approaches to the treatment of charge transfer. We then review the EAM method and describe previous attempts to adapt the model to the study of charge-transfer systems. This is followed by a summary of the key features of the recently proposed CT-EAM as implemented in the present work. In Section III, we present our potential parameterization, and in Section IV, the results of the model for various water clusters. The paper concludes with a summary and discussion of future work.

II. BACKGROUND

A. Water potentials

Understanding the thermodynamic and structural properties of water is crucial to modeling many biological, chemical and physical phenomena. Despite its relevance and importance, there are still unanswered questions regarding the properties of water polymorphs and their exact roles in solution chemistry as well as in biological processes. Developing an accurate model capable of simultaneously describing the gas phase, liquid, and solid state properties of water has presented enormous challenges. Ultimately, a complete model should be capable of describing diverse phenomena such as ion solvation,[22] electro-,[23] photo-,[24] and thermo-[25] dissociation of water; dynamical properties of the liquid,[26,27] and anomalous thermodynamics.[28]

There have been many previous attempts to develop potentials capable of describing the various phases and properties of water, with varying degrees of success. Comprehensive reviews are available in Refs. [29,30], and we will not attempt to review the potentials in detail, but rather highlight essential features. Most have concentrated on describing liquid water properties such as the temperature-density variation, second virial coefficient, diffusivity, radial distribution functions and structure functions; others have focused on accurately reproducing gas-phase spectrosocopic data.[31] Some of the best-known potentials are essentially empirical in nature (ST2,[32] SPC,[33] SPC/E,[34] TIP3P,[35] TIP4P,[36] TIP5P[37]), while others have used *ab initio* calculations carried out on small water clusters (monomer, dimer) for their parameterizations (MCDHO,[38] SAPT,[39] NCC,[40,41] MCY,[42] NEMO,[43] CC-pol[44]) or a combination of *ab initio* and experimental data (POL5,[45] DIM water[46]). In almost all of the potentials, the parameterizations are carried out with the implicit assumption that the basic structural unit consists of the water monomer/molecule (notable exceptions being Halley *et al.*,[47] Corrales,[48] and Voth *et al.*[15,22]) Typically, the molecule is represented by a collection of point charges placed at suitable sites so as to yield the correct dipole and higher multipole moments for liquid water, as well as the structures of small water clusters in some cases. The total energy of a system comprised of water molecules is expressed as a sum of coulombic and non-coulombic terms. Simpler potentials hold the geometry of the water molecule as well as the values of the point charges fixed[33,35,36,37,49] while more realistic potentials allow OH bond flexibility, modeled as harmonic and anharmonic oscillators.[50,51] Further, rigid molecule models like that of Dang and Chang,[52] ASP,[53] and NEMO[43] include polarization effects by accounting for induced dipole moments at every atom site in a self-consistent manner, while potentials like TIP4P-FQ[26] use an approach similar to ES+[5] (see Section II.B) to account for polarization. Other potentials that account for polarization effects include MCDHO,[38] which uses a three-site model in addition to a negative mobile charge corresponding to a polarized electron cloud, the diffuse charge pair potential model of Guillot and Guissani,[54] Polarflex,[27] based on empirical valence bond theory, and TTM,[55] which uses smeared charges and dipoles.

B. The embedded-atom method and charge-dependent extensions

The EAM formulation and extensions such as MEAM have been used to successfully model a wide range of condensed phase systems, including *fcc* metals,[56] binary alloys,[57,58] tin,[59] group IV elements such as Si,[10] and even organic polymers.[60] In the basic method, the total cohesive energy of a system is expressed as a function of a local electron density, with each atom viewed as an impurity embedded in a host consisting of the remaining atoms. The host electron gas provides both ion-ion interactions and a volume-dependent energy component.[7]

The total energy of the system is written as follows:

$$E_{\mathrm{EAM}} = \sum_{i=1}^{N} E_i, \tag{1}$$

where N is the number of atoms and

$$E_i = F_i(\overline{\rho}_i) + \frac{1}{2}\sum_{j\neq i}\phi_{ij}(R_{ij}). \tag{2}$$

F_i is an element-dependent *embedding function* of the effective local electron density $\overline{\rho}_i(\mathbf{R}_i)$ at atomic site i, and represents the collective many-body effects of the remaining atoms in the host material; ϕ_{ij} corresponds to a pair potential between interacting atoms i and j. The inclusion of the many-body term F_i in the energy expression makes the EAM significantly different from traditional two-body potentials. Moreover, in contrast to earlier approaches that utilized bulk volume corrections, the EAM volume dependence is local to each atom,[8] corresponding to an effective dependence on local coordination.[61] Equivalently—in a tight-binding bond picture of the EAM—the embedding energy can be understood in terms of a local moment approximation to the density of states.[62]

In the simplest EAM formulation, parameterized isolated-atom electron densities are associated with each nucleus, and $\overline{\rho}_i(\mathbf{R}_i)$ is approximated by the sum of the tails of all neighboring atom electron densities at site i:

$$\overline{\rho}_i(\mathbf{R}_i) \simeq \sum_{\substack{j=1\\ j\neq i}}^{n_i} \rho_j^a(\mathbf{R}_{ij}). \tag{3}$$

Here n_i is the number of nearest neighbors of atom i, and ρ_j^a corresponds to the isolated atomic electron density of neighbor j. Various refinements of $\overline{\rho}_i$ have been devised to account for neutral electron density polarization[10,63,64] as well as the inclusion of alloying effects.[58]

As noted in the Introduction, EAM-based potentials in their original formulation do not account for explicit charge dependence or charge transfer. To address this limitation in their models of metal-oxide systems, Streitz and Mintmire[5] proposed an extension of EAM, ES+, in which an electrostatic energy term E_{es} was added to E_{EAM}. E_{es} is defined by the equation

$$E_{es} = \sum_{i=1}^{N} {E_i}^{\mathrm{ion}}(q_i) + \frac{1}{2}\sum_{\substack{i,j=1\\ i\neq j}}^{N} V_{ij}, \tag{4}$$

where ${E_i}^{\mathrm{ion}}(q_i)$ represents the ionization energy of an isolated atom i, q_i is its charge, and V_{ij} is the coulomb interaction energy. Following the Rappé and Goddard QEq model,[65] ${E_i}^{\mathrm{ion}}(q_i)$ is expressed in terms of atomic charge q_i, atomic electronegativity χ_i^0, and atomic hardness J_i^0 via a second order Taylor series expansion about the isolated neutral atom energy ${E_i}^{\mathrm{iso}}(0)$:

$${E_i}^{\mathrm{ion}}(q_i) = {E_i}^{\mathrm{iso}}(0) + \chi_i^0 q_i + \frac{1}{2}J_i^0 q_i^2. \tag{5}$$

In addition, V_{ij} is expressed in terms of effective electron densities ϱ_i and ϱ_j of atoms i, j as

$$V_{ij} = \int\int \frac{\varrho_i(\mathbf{r}, q_i; \mathbf{R}_i)\varrho_j(\mathbf{r}', q_j; \mathbf{R}_j)}{|\mathbf{r}-\mathbf{r}'|}\, d\mathbf{r}\, d\mathbf{r}', \tag{6}$$

where $\mathbf{R}_i$ and $\mathbf{R}_j$ are the position vectors of the atomic nuclei, and q_i and q_j are the atomic charges. The ϱ_i include screened nuclear and polarized valence electron components. The latter are modeled using a shape function f_i with a fixed (optimized) parametric form. The instantaneous charge on each atom, which varies as a function of atomic configuration, is obtained via chemical potential equalization, and requires the solution of N coupled linear equations involving the V_{ij} and a set of charge- and interaction-dependent electronegativities χ_i.

The original Streitz-Mintmire formulation was used to represent atomic interactions in the Al-O system, and correctly predicted elastic and energetic properties in the bulk, as well as surface energies and relaxations, with reasonable assignments of ionic charges for the Al and O atoms.[5,6] It was later used successfully in dynamical simulations of the energetics of vacancies in γ-alumina[66] and in studies of the oxidation of aluminum nanoclusters,[67] again with reasonable values for the computed ionic charges. However, Zhou *al.* noted that the model could not describe the behavior of the α phase of Al_2O_3 under compression, wherein the computed charges oscillated between large unphysical values at short interatomic spacings.[68] This behavior was attributed to a compensating effect on the part of the EAM component of the ES+ potential, whose particular parameterization effectively constrained the atoms from approaching too closely. To address this problem, and also enable the use of alternative EAM parameterizations within ES+, Zhou *et al.* developed a variant in which *a priori* empirical charge bounds were imposed on the ions in the electrostatic component. The resulting CTIP-EAM model successfully described cohesive and surface energies, surface oxidation, and thin-film growth of various Al/Zr-oxide systems.

A primary limitation of both ES+ and CTIP-EAM is that they assume a quadratic Taylor series expansion about the nominal ionic charges and are thus valid only for reasonably small fluctuations about these values.[17,18] This precludes a non-perturbative description of charge transfer in reactive systems, and the significant electron density rearrangements that are induced by strong intermolecular interactions. It also prevents a proper description of the dissociation of interacting atomic and molecular species, since the imposed quadratic dependence on charge does not transition smoothly to the correct linear dependence at long range.[69,70,71]

A second pressing issue is the lack of self-consistency in both ES+ and CTIP-EAM, since the $\varrho_i(\mathbf{r}, q_i; \mathbf{R}_i)$ appearing in the electrostatic component of these potentials is regarded as formally distinct—and is parameterized separately from—the EAM electron density ρ_i^a. This must be regarded as problematic in light of the intrinsic

long-range, many-body nature of charge polarization and charge transfer. At the electronic level, it is well known that subtle interactions in the vicinity of quantum mechanical curve crossings,[74] and the concomitant interplay between short and long-range electronic correlations, can have a profound effect on the details of chemical bonding. Indeed, such effects in water have been recently the focus of considerable theoretical and experimental interest.[75] Both the problem of significant charge polarization as well as the self-consistency issue in ES+ have been noted previously in the context of alumina.[76] At the atomistic level, these intrinsically quantum mechanical effects must be properly reflected in the design of the potential if it is to accurately describe charge transfer and reactive dynamics.

C. Charge-transfer embedded atom method potential for water

A potential that addresses both of these issues within a density functional-based multiscale formalism has been developed recently.[17,18] The formalism unifies all extant embedded-atom models within a common theoretical framework, and as an immediate consequence, generalizes to a fully-interacting, self-consistent charge-transfer embedded-atom potential. This potential is used here as the starting point for constructing a new charge-transfer potential for water.

For details, we refer the reader to the original papers. Here we summarize the central results. First, we note that the formalism automatically imposes the requirement that ρ equal ϱ in the embedding and electrostatic components of the potential, and incorporates a proper treatment of the long-range dissociation of interacting subsystems.[71,72] These constraints together effect the crucial balance between short- and long-range electronic correlations.

The general CT-EAM form has been shown to be derivable from the exact quantum-chemical atom-in-molecule (AIM)[77] and diatomics-in-molecule (DIM)[13] Hamiltonians. In this picture, charge-transfer-dependent embedding functions correspond to one-atom AIM terms, while pair potentials map onto two-atom DIM terms.[17] This reformulation suggests a practical approach to the parameterization of CT-EAM molecular potentials based on resonance state (diabatic charge state) potential curves.[73] Here, we adopt the parameterization perspective of Refs. [18,71,72], which emphasizes the charge-transfer electron densities as fundamental variables. Regardless of which approach is chosen, however, two key elements of the original theory must be modified: the form assumed by the background embedding densities, and the total cohesive energy expression.

Consider the background embedding density first. We begin by decomposing the total electron density into a sum of AIM components, denoted by $\rho_i^*(\mathbf{r};\mathbf{R}_i)$. Here $\mathbf{r}$ represents an arbitrary point in space for the electronic coordinate, and the ρ_i^*'s are assumed centered on the corresponding atomic nuclei. The ρ_i^* play an analogous role in CT-EAM to the isolated electron densities ρ_i^a in the original EAM. We use 'atom-in-molecule' as a general term for referring to the ρ_i^*, whether derived from molecules, clusters, or solids. In principle, any physically-justified AIM decomposition can be used.[77,78] The sole requirement is that the decomposition satisfy $\rho(\mathbf{r};\mathbf{R}) = \sum_i \rho_i^*(\mathbf{r};\mathbf{R}_i)$, where $\mathbf{R} = \{\mathbf{R}_j\}$ is a collective variable representing the instantaneous geometry of all atoms in the system.

The CT-EAM forms for the background embedding densities and effective atomic charges q_i are obtained as appropriate weighted averages of the density difference

$$\Delta_i(\mathbf{r};\mathbf{R}) = \rho(\mathbf{r};\mathbf{R}) - \rho_i^a(\mathbf{r};\mathbf{R}_i)\,. \tag{7}$$

Δ_i corresponds to the electron density distribution of the medium in which the ith atom is embedded. Let χ_i^L be a weight function yielding the spatially-averaged quantity Θ_i^L:

$$\Theta_i^L = \int \Delta_i(\mathbf{r};\mathbf{R})\,\chi_i^L(\mathbf{r})\,d\mathbf{r}\,. \tag{8}$$

If χ_i^L is constructed so as to project out $\rho_i^*(\mathbf{r};\mathbf{R}_i)$ from $\rho(\mathbf{r};\mathbf{R})$, we obtain a uniform average of the density difference between ρ_i^* and ρ_i^a, which is simply the effective charge:

$$q_i = \int \left(\rho_i^*(\mathbf{r};\mathbf{R}_i) - \rho_i^a(\mathbf{r};\mathbf{R}_i)\right)\,d\mathbf{r}\,. \tag{9}$$

q_i is the *localized* zeroth order moment ($L = 0$) of $\Delta_i(\mathbf{r};\mathbf{R})$. Note that this relation formally connects the AIM densities and effective charges. This is the mechanism through which CT-EAM imposes its requirement on the embedding and electrostatic components of the potential, that $\rho = \varrho$.

If instead we take χ_i^L equal to a δ-function centered on atom i, and utilize the density decomposition of $\rho(\mathbf{r})$, we obtain an expression for the embedding density $\overline{\rho}_i^*$:

$$\begin{aligned}
\overline{\rho}_i^*(\mathbf{R}_i) &= \int \left[\rho(\mathbf{r};\mathbf{R}) - \rho_i^a(\mathbf{r};\mathbf{R}_i)\right]\delta(\mathbf{r}-\mathbf{R}_i)\,d\mathbf{r} \\
&\approx \int \left[\rho(\mathbf{r};\mathbf{R}) - \rho_i^*(\mathbf{r};\mathbf{R}_i)\right]\delta(\mathbf{r}-\mathbf{R}_i)\,d\mathbf{r} \\
&\approx \sum_{j\neq i} \rho_j^*(\mathbf{R}_{ij}).
\end{aligned} \tag{10}$$

In the second step, we have approximated ρ_i^a by ρ_i^*. This is reasonable because for purposes of estimating the embedding density, the difference between the isolated and AIM densities for the atom experiencing the embedding is comparatively small. Most contemporary EAM calculations already implement a similar approximation: parameterized functional forms for the ρ_j^a's in Eq. (3) are included within the overall potential specification, and thus effectively serve as AIM ρ_j^*'s.

In light of Eq. (10), the CT-EAM background embedding density $\overline{\rho}_i^*(\mathbf{R}_i)$ at atom i corresponds to the localized infinite moment ($L = \infty$) of $\Delta_i(\mathbf{r};\mathbf{R})$. q_i and $\overline{\rho}_i^*(\mathbf{R}_i)$ are thus closely related, each expressible as a distinct localized moment of $\Delta_i(\mathbf{r};\mathbf{R})$.

The second modification of the EAM concerns the cohesive energy expression. The CT-EAM generalization of Eqs. (1)-(2) is[17,18]

$$E = \sum_i \left[\sum_{M=1}^{M_i} \Omega_{i,M} F_{i,M}[\overline{\rho}_{i,M}^*] + \frac{1}{2} \sum_{j \neq i} \sum_{M=1}^{M_{ij}} \Omega_{ij,M} \Phi_{ij,M} \right]. \tag{11}$$

In the embedding term, the index M sums over the M_i integer charge states that are to be included in the model for the ith atom; in the pair interaction term, M sums over all M_{ij} *pairs* of included charge states. $F_{i,M}$, $\Phi_{ij,M}$ and $\overline{\rho}_{i,M}^*$ are charge-transfer generalizations of the conventional EAM quantities. The $\Omega_{i,M}$ and $\Omega_{ij,M}$ are weighting factors for the particular integer charge states or combinations of charge states that are instantaneously populated for a given system configuration.

In order to make practical use of the CT-EAM formulation, it is necessary to choose the number of charge states to be included for each atom type, and also the parametric functional forms to be used for the embedding functions $F_{i,M}$ and pair interactions $\Phi_{ij,M}$. These choices are discussed below in Section III.

III. CT-EAM POTENTIAL FOR WATER

An obvious concern with the fixed-charge models is that they lack the flexibility to describe phenomena where the neutral water molecule is not necessarily the fundamental structural unit. Even more sophisticated approaches such as MEVB and SAPT associate charges with fixed molecular and ionic species (water, hydronium ion). Additionally, they rely on the specification of appropriate quantum-mechanical basis states in order to compute dynamical charges. These features make such models difficult to generalize to the study of larger and more complex water-containing systems where charge transfer effects are expected to play a significant role. Important examples include the dynamics of solvated proteins,[79] water-silica interactions,[80] energy transduction in molecular motor proteins,[81] and the electronic and magnetic properties of exotic materials.[82]

The use of the EAM as the starting point of our approach means that our perspective is shifted from larger molecular building blocks to a more fine-grained picture—exact in DIM—of perturbed atoms embedded in a many-body medium, and explicit two-body interactions. The formal basis for the methodology in density functional theory implies that CT-EAM potentials are in principle capable of describing arbitrary charge states and energetics of the atoms in any given local chemical environment.

Using Eq. (11) as our starting point, we will now develop an environment-dependent potential that is parameterized to reproduce the ground-state energy and geometry of the water monomer and dimer for select geometries of these structures. The parameterization incorporates charge transfer information derived from *ab initio* calculations on the hydronium and hydroxyl ions, the neutral isolated water molecule, and neutral water dimer.

A. Environment-dependent atomic charges

In principle, the CT-EAM potential should be formulated in terms of AIM electron densities and a relatively complete set of atomic charge states, as outlined in the previous section. In this first application of the theory, however, our aim is to explore the capabilities of the framework in the simplest possible implementation. We therefore adopt the AIM atomic charge as a surrogate for the background density at a given atomic site; ultimately, it will be necessary to utilize more detailed approximations of the AIM spatial distributions, particularly for dynamical simulations. As is clear from the discussion surrounding Eqs. (9)–(10), this approximation is equivalent to replacing the electron density distribution by its localized zeroth order moment. We also assume two charge states per atom, as discussed below.

Given the functional form for the CT-EAM energy (Eq. (11)), our first task is to develop appropriate parameterizations for the atomic charges q_i. The dataset used to fit the AIM charges is computed using standard population analysis techniques in conjunction with *ab initio* calculations. We have used the *ab initio* software package `GAMESS`[83] at the unrestricted Hartree-Fock (UHF) level and with a fairly high-quality basis set—6-31G**—to obtain the Löwdin atomic charges.[84] The same basis set and level of theory were used in all parameterization calculations throughout this work, and all charge and potential parameters were varied in order to limit model estimation errors to less than 0.015 e and 0.02 eV per molecule, respectively. Although electron correlation and other effects such as zero-point energy corrections are not included in these calculations, Maheshwary *et al.* have performed extensive *ab initio* calculations on water clusters using HF/6-31G** and concluded that overall trends in the variation of energy with cluster size remained unaltered with further improvements in basis set and level of theory.[86] Indeed, comparison of their results with recent accurate X3LYP hybrid density functional energies, computed with a much larger aug-cc-pVTZ(-f) basis set,[87] reveals a nearly identical pattern of variation in stabilization energy for the most stable geometry of $(H_2O)_n$ as a function of cluster size n. As our model systems we choose different geometries of: i) the neutral water molecule, ii) the hydronium ion H_3O^+, iii) the OH^- ion, and iv) the water dimer, in order to represent diverse coordination environments. It is important to bear in mind that these structures and geometries are used here

to parameterize charge rather than energy. We therefore expect electron correlation effects to be less important than the quality of the basis set.

The motivation behind using different model systems is to ensure that the resulting interatomic potential is sufficiently robust to describe different chemical environments that the oxygen and hydrogen atomic species might encounter in various water polymorphs. The particular choice of the H_3O^+ and OH^- ions is based on two key considerations. First, they provide a coordination environment for the hydrogen and oxygen atoms that is distinct from neutral interacting H_2O dimers. Second, H_3O^+ and OH^- are the two primary dissociation products of water in solution, and thus are essential to describing chemical reactions involving water.

A distinguishing feature of our methodology is the identification of *local clusters* within an instantaneous configuration of the system, and the indexing of an atom's charge based on the kind of cluster to which it belongs. Each local cluster is assigned a charge depending on the number of atoms in the cluster, with the charge partitioned among the cluster atoms in a geometry-dependent manner. For each oxygen atom, we identify the number of hydrogen atoms within a radius that is chosen to be 1.5 Å. For example, if two hydrogen atoms are in close proximity to an oxygen atom, then the cluster (oxygen plus two hydrogen atoms) constitutes a neutral H_2O cluster, while if the number of hydrogens surrounding an oxygen atom is three, then the cluster is identified as a H_3O^+ with a net cluster charge of +1. The total charge on an identified cluster with $N_{\rm H}$ hydrogen atoms is thus $N_{\rm H} - 2$. Once all clusters have been identified, the total cluster charge is partitioned among the atoms as a function of their relative positions within the cluster. We then account for further charge polarization and charge transfer between neighboring clusters by parameterizing the amount of charge transferred between two water monomers (constituting a dimer) as a function of the hydrogen-bond distance between the two monomers. The final total charge on a given atom consists of both intra-cluster and inter-cluster contributions; this corresponds to its effective AIM charge. The following section provides further details of the charge parameterization procedure.

B. Model Clusters: H_2O, H_3O^+, and OH^-

For the three model clusters, we initially obtained the equilibrium geometries as given in Table I. Next, we varied the geometries of the three systems to obtain the Löwdin atomic charges as a function of system geometry as shown in Fig. 1. For the water molecule, atomic charges for the three vibrational modes (symmetric stretch, asymmetric stretch, and bending) were obtained, and the charges were fitted as a function of the two OH bond distances and the intramolecular angle. The symmetric and asymmetric stretches and contractions varied from 70% to 140% of the equilibrium bond length (R_{eq}) at various values (55%–130%) of the equilibrium intramolecular angle (θ_{eq}). In a similar fashion, we obtained charges for symmetric deformations (70% to 140%) of the OH bonds with the three bond angles fixed at the equilibrium value for the H_3O^+ ion as well as the Löwdin charges on the O and H atoms for the OH^- anion for deformations ranging from 70% to 140% of the equilibrium OH bond distance. We then fitted the atomic charge variations as a function of the relative positions of the respective atoms in the cluster.

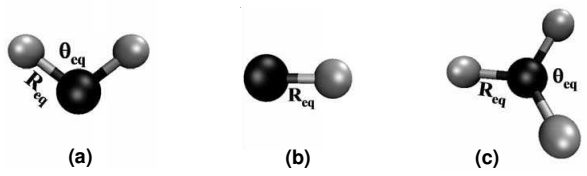

FIG. 1: Geometry of the three model clusters: (a) H_2O; (b) OH^-; (c) H_3O^+.

TABLE I: Equilibrium geometry values for the model clusters. Angles in degrees; distances in Å.

	θ_{eq}	R_{eq}
OH^-	—	0.958
H_2O	105.5	0.945
H_3O^+	114.74	0.961

We now present the parameterization equations relating the variation in atomic charge with respect to cluster geometry. As noted previously, the number of atoms in a cluster is defined by a central oxygen and the number of hydrogen atoms that lie within a specified radial cutoff $r_{cut} = 1.5$ Å.

Consider a cluster with a central oxygen O and $N_{\rm H} > 1$ hydrogen atoms. Let the position vector of the p^{th} hydrogen atom with respect to the central oxygen atom O be $\mathbf{r}_p$. The charge $q^p_{\rm H}$ on the p^{th} hydrogen atom is expressed as a function of the positions of all atoms in the cluster, specifically, $\theta_{p{\rm O}s}$, r_p and r_s, where s corresponds to any of the other $N_{\rm H}-1$ hydrogen atoms in the cluster, $\theta_{p{\rm O}s}$ is the angle between $\mathbf{r}_p$ and $\mathbf{r}_s$, and r_s is the distance of the s^{th} hydrogen atom from O. We have

$$q^p_H = q^p_1 + q^p_2 + q^p_{N_{\rm H}>2}, \tag{12}$$

where

$$q^p_1 = \sum_{\substack{s=1\\ s\neq p}}^{N} \Big[\alpha(\theta_{s{\rm O}p})e^{-2r_p} + \beta(\theta_{p{\rm O}s})r_p e^{-r_p} + c(\theta_{p{\rm O}s})\Big] \sin^2\theta_{p{\rm O}s}, \tag{13}$$

$$q^p_2 = \sum_{\substack{s=1\\ s\neq p}}^{N_{\rm H}} (r_p - r_s) d(\theta_{p{\rm O}s}) \sin^2\theta_{p{\rm O}s}, \tag{14}$$

TABLE II: Water monomer charge model parameters I.

α_1 (e)	α_2 (e)	β_1 (e)	β_2 (e/Å)	γ_1 (e)	γ_2 (e)	t_1 (Å)
−10.032	9.3087	7.7183	3.0558	−1.4124	−6.7189	0.03

and

$$q^p_{N_{\rm H}>2} = \sum_{\substack{s=1 \\ s\neq p}}^{N_{\rm H}} \left[\alpha_2 e^{-2r_p} + \beta_2 r_p e^{-r_p} + \gamma_2 e^{-r_p}\right] \sin^2\theta_{pOs}. \tag{15}$$

$q^p_{N_{\rm H}>2}$ is non-zero when $N_{\rm H} > 2$. α β, c, d are functions of θ_{pOs}, defined in Eqs. (20)–(23) below; α_2, β_2, and γ_2 are constants whose values are given in Table II. For the special case where the identified cluster contains only a single hydrogen, the charge on the hydrogen is given by

$$q^p_{\rm H} = \alpha_1 e^{-2r_p} + \beta_1 e^{-r_p} + \gamma_1, \tag{16}$$

where α_1, β_1, and γ_1 are constants specified in Table II.

To prevent energy discontinuities, we utilize a switching function $\mathcal{S}(t)$ to modulate the calculated charge on hydrogen atom p as a function of r_p:

$$\tilde{q}^p_{\rm H} = q^p_{\rm H}\ \mathcal{S}(r_p - t_{cut}), \tag{17}$$

where

$$\mathcal{S}(t) \equiv \frac{1}{2}\Big(1 - \tanh(t/t_1)\Big). \tag{18}$$

Here $q^p_{\rm H}$ is given by Eq. (12) or Eq. (16) depending on the oxygen coordination, $t_{cut} = 1.41$ Å, and t_1 is given in Table II. The role of $\mathcal{S}$ is to asymptotically switch $\tilde{q}^p_{\rm H}$ from $q^p_{\rm H}$ to zero at a radius that is less than the cluster assignment cutoff r_{cut} (note that $t_{cut} < r_{cut}$). This prevents energy discontinuities when an H crosses from outside to inside the r_{cut} boundary. Depending on the number of hydrogen atoms $N_{\rm H}$ in the cluster, the charge $q_{\rm O}$ on the oxygen atom in the cluster is

$$q_{\rm O} = (N_{\rm H} - 2) - \sum_{p=1}^{N_{\rm H}} \tilde{q}^p_{\rm H}. \tag{19}$$

The functional forms for α, β, c and d are given by the following equations (parameters are listed in Table III):

$$\alpha(\theta) = a_1 e^{\theta} + a_2 e^{\theta^2/4} + a_3\theta, \tag{20}$$

$$\beta(\theta) = b_1\theta e^{-\theta} + b_2\theta e^{-2\theta} + b_3\theta^2, \tag{21}$$

$$c(\theta) = c_1\theta e^{-\theta} + c_2\theta e^{-2\theta} + c_3, \tag{22}$$

$$d(\theta) = d_1(\theta - \theta^2) + d_2\theta^3. \tag{23}$$

Fig. 2 compares the actual and predicted charges for the oxygen atom in the three different clusters for select geometries. The fits are very good in each case.

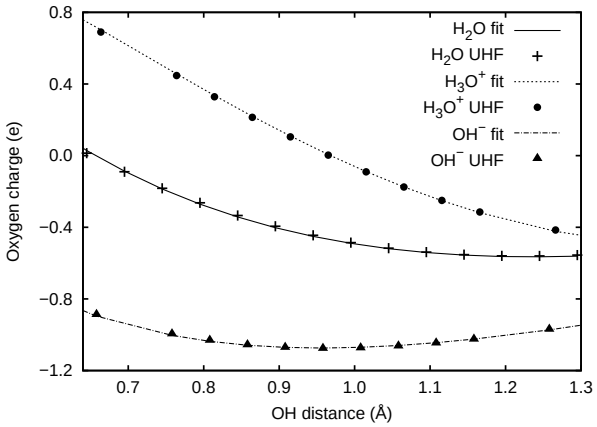

FIG. 2: Oxygen charge as a function of OH distance for a symmetric variation at θ_{eq} in H_2O, H_3O^+, and OH^-.

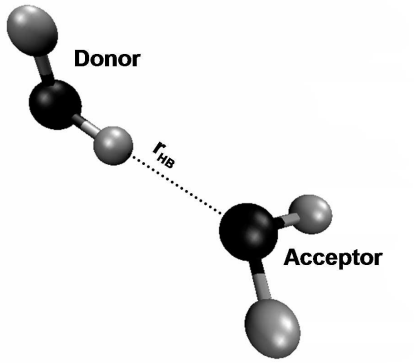

FIG. 3: Water dimer geometry, illustrating hydrogen bonding.

C. Charge Transfer between Clusters: Water Dimer Atomic Charges

Water polymorphs are characterized by the formation of hydrogen bonds between neighboring water molecules. Thus, the environment of any atom in bulk is different than when it is part of an isolated water molecule. In order to include the effect of a bulk environment on the atomic charges, we considered two water molecules (dimer) and parameterized the atomic charges for select geometries of the dimer (see Fig. 3). This was done by fixing the geometries of the individual water molecules to match the equilibrium isolated water geometry and moving the two molecules relative to each other along the line of hydrogen bonding $\mathbf{r}_{\rm HB}$ between the two molecules.

Using the same level of theory as above, the equilibrium dimer geometry was computed, yielding intramolecular bond distance and bond angles of 0.950 Å and 105.5°, respectively. The computed intermolecular hydrogen bond distance $r_{\rm HB}$ was 2.03 Å, with an intermolecular bond angle φ (formed between the two oxygens and the common hydrogen; see Fig. 6) of 172.3°.

TABLE III: Water monomer charge model parameters II.

a_1 (e)	a_2 (e)	a_3 (e)	b_1 (e)	b_2 $(e/\text{Å})$	b_3 $(e/\text{Å}^2)$	c_1 $(e/\text{Å}^2)$	c_2 $(e/\text{Å}^3)$	c_3 $(e/\text{Å}^3)$	d_1 $(e/\text{Å})$	d_2 $(e/\text{Å})$
0.8158	−3.2198	0.5725	−14.0058	61.8232	1.3188	12.2353	−15.7797	−3.5928	0.4430	0.1154

Note that the equilibrium intramolecular bond distances and angles for each molecule are very similar to those of a single water molecule, while the intermolecular angle corresponds to a nearly linear configuration.

We next varied r_{HB} from 75% to 130% of its equilibrium value, keeping the geometry of the two molecules rigid and fixing φ at its equilibrium value. This resulted in a finite intermolecular charge transfer between the two molecules, such that the donor molecule became negatively charged relative to the acceptor molecule as a function of the common hydrogen position. Based on these results, we defined a net intermolecular charge transfer dq (donor $\rightarrow$ acceptor) between the two clusters, and a partitioning—referred to collectively as $\{dq_i\}$—of this charge transfer among the constituent atoms. dq is parameterized as:

$$dq = a_{im} e^{-b_{im} r_{\text{HB}}}, \tag{24}$$

where r_{HB} is the distance between the donor hydrogen and acceptor oxygen. Based on our HF calculations, we choose the cutoff for charge transfer between clusters to be $s_{cut} = 2.5$ Å (beyond this distance the computed dq was effectively zero.) As above (*cf.* Eq. (17)), the switching function $\mathcal{S}$ modulates dq so as to ensure energy continuity; it guarantees that if $r_{\text{HB}} > s_{cut}$, there is no intermolecular charge transfer:

$$d\tilde{q} = dq\ \mathcal{S}(r_{\text{HB}} - r_{qim}). \tag{25}$$

The parameters a_{im}, b_{im}, and r_{qim} in Eqs. (24) and (25) are given in Table IV. $d\tilde{q}$ is partitioned among the atoms as follows:

$$dq^{\text{O}_{donor}} = -0.5\, d\tilde{q} \tag{26}$$

$$dq^{\text{O}_{acceptor}} = 0.75\, d\tilde{q}, \tag{27}$$

and

$$dq^{\text{H}_{donor}} = -0.4\, d\tilde{q}, \tag{28}$$

where O_{donor}, $\text{O}_{acceptor}$, and H_{donor} represent the donor oxygen, acceptor oxygen, and donor hydrogen respectively. For the acceptor molecule, $dq^{\text{H}_{acceptor}}$ is computed by partitioning $[d\tilde{q} - dq^{\text{O}_{acceptor}}]$ equally among the constituent hydrogens in that cluster. Similarly, $[(dq^{\text{O}_{donor}} + dq^{\text{H}_{donor}}) - d\tilde{q}]$ is distributed equally among the hydrogen atoms (other than H_{donor}) in the donor cluster. The total charge q_i on the ith atom is given by

$$q_i = q_i^{cl} + dq_i, \tag{29}$$

TABLE IV: Water dimer charge model parameters.

a_{im} (e)	$b_{im}(\text{Å}^{-1})$	r_{qim} (Å)
1.5812	1.8222	2.35

where q_i^{cl} is the atomic charge due to intramolecular charge transfer, calculated from Eqs. (12)–(19) ($q_i^{cl} = q_{\text{H}}^p$ for H, and q_{O} for O), and dq_i is the additional atomic charge acquired via intermolecular charge transfer (Eqs. (24)–(28)). As we shall see shortly, all three values—q_i, q_i^{cl}, and dq_i—are needed for computing the total energy in CT-EAM. q_i^{cl} and dq_i are the background density arguments to distinct charge transfer embedding functions (see Section III.D), and q_i is used to compute the coulomb pair interaction energy.

The specification of the CT-EAM charge transfer parameterizations for both intra- and inter-cluster interactions is now complete. Note that we have assumed that each cluster is defined such that a given H atom belongs to only one cluster. In particular, the identification of a 'hydrogen-bonding' H atom implicitly assumes that the H atom belongs to one cluster and is hydrogen-bonded to the oxygen of the neighboring cluster.

There are a number of special cases that may arise; these are handled as follows. If a hydrogen belongs to more than one cluster, we initially treat the clusters separately, account for their cluster charges, and add the respective contributions for the common hydrogen. Then we use the inter-cluster charge transfer function to determine the charge transfer between the two clusters in each direction, and add the results. That is, for the given pair of clusters, we consider both scenarios where one cluster acts as a donor and the other as an acceptor and vice-versa. If more than one donor hydrogen is shared between two clusters, we use the same set of charge transfer equations to compute two sets of charge transfers between the clusters: there is no coupling between them. Finally, the charge transfer between clusters is always mediated by the *hydrogen* atoms, irrespective of the relative distances between the corresponding oxygens.

D. Charge-dependent embedding functions

We have described two intrinsic types of charge transfer in the water system—inter- and intra-molecular—and presented parameterizations for each. These two types of charge transfer make distinct contributions to the energy through their respective charge-state-dependent embedding functions (*cf.* Eq. (11)). We must now consider

how to determine appropriate functional forms for these embedding functions.

In the original EAM formulation, the atomic embedding functions were determined by numerical fits of the energy to configurational reference states along a symmetric dilatation curve.[9] Later, as a key aspect of MEAM, Baskes proposed the use of a universal $\rho \ln \rho$ functional form, with the density argument normalized to a reference state. Baskes rationalized this form by noting that it gave the correct coordination dependence between bond length and energy (bond-order/bond-length correlation) for Si.[10] Indeed, MEAM has since proved remarkably robust in applications to chemically-diverse materials systems.[9,10,57,59] This suggests that the same form may also work well as an *ansatz* for the charge-transfer embedding functions required here.

An independent rationale for the $\rho \ln \rho$ form comes from recent work on ensemble models of charge transfer for strongly-interacting subsystems.[71] In a resonance-state (microscopic) ensemble picture, the equilibrium charge transfer within a larger closed system provides a measure of the interaction strength between subsystems. In the equivalent thermodynamic ensemble, the charge transfer parameter maps onto a *non-zero* electronic temperature. This temperature is conjugate to the charge-density entropy induced by the electronic polarization and charge transfer among constituent subsystems. Interpreting the charge transfer in terms of an effective electronic temperature suggests using the information-theoretic form of the entropy ($\sum_i \rho_i \ln \rho_i$, where i indexes the pure states contributing to the ensemble[70]), to model the charge-transfer embedding energies.

In light of the universal nature of the density functional electronic theory underlying CT-EAM, we expect the embedding functional form to be independent of the nature (inter- or intra-molecular) of the charge transfer. We therefore adopt the $\rho \ln \rho$ form for all charge-transfer embedding functions—using charges instead of background densities as discussed below. Finally, the ensemble formulation and information-theoretic interpretation both suggest that distinct charge transfer contributions should enter additively into the overall energy expression; this is consistent with the formal result in Eq. (11).

E. Embedding function and pair interaction parameterizations

The parameterizations we have chosen for the AIM charges imply a choice of $M_i = 2$ for both H and O, and $M_{ij} = 3$ for the pair interactions (Eqs. (33)–(35)). We write the net embedding energy contribution F_i of the ith atom in terms of q_i^{cl} and dq_i as:

$$F_i = A_i q_i^{cl} \ln(e_0 {q_i^{cl}}^2) + A_i^d dq_i \ln(e_0 {dq_i}^2), \qquad (30)$$

where $e_0 = 1$ has dimensions of e^{-2}. We use the square of the charge to ensure a positive argument for the logarithm; the additional factors of two are absorbed into the parameterization via the prefactors. The intra- and interatomic charge transfer values q_i^{cl} and dq_i are used in lieu of the nominal background embedding densities $\overline{\rho}^*_{i,M}$, $M = 1{,}2$. The justification for this comes from the common origin of q_i and $\overline{\rho}^*_i$ in Eq. (8). We have also absorbed the weighting factors $\Omega_{i,M}$ and $\Omega_{ij,M}$ into our parameterizations (Eqs. (30)–(35)).

Further insight into Eq. (30) can be obtained by regarding the first term as corresponding to conventional EAM, with the AIM charges within the water monomer playing the role of the embedding electron density. This term is associated with first-neighbor, intra-molecular charge transfer. The second term is then a CT-EAM correction for second nearest-neighbor, inter-molecular charge transfer. It is interesting to note in this connection that a second-nearest-neighbor MEAM has been proposed recently, aimed at correcting the structural stability and surface energy orderings in certain *bcc* metals.[92]

The total pair interaction Φ_{ij} is given by the sum of two terms, a classical electrostatic component, V_{ij} (analogous to Streitz and Mintmire's V_{ij}, *cf.* Eq. (4)), and a *non-coulombic* component, ϕ_{ij} (*cf.* Eq. (2)):

$$\Phi_{ij} = V_{ij} + \phi_{ij}. \qquad (31)$$

Since we have chosen to utilize localized zeroth-order moment models of the AIM electron densities, the electrostatic component of Φ_{ij} consists simply of the classical coulombic interaction between AIM charges q_i and q_j,

$$V_{ij} = q_i q_j / R_{ij}. \qquad (32)$$

These charges are constrained to be identical to those appearing in the embedding component of the potential, in accordance with the CT-EAM self-consistency requirement. The form of the non-coulombic potential is dictated by energy fits once the charge-dependent components have been determined. These assume a purely repulsive Born-Mayer-type form for the homonuclear pair interactions, and a linear-exponential form for the OH interaction. They are similar to the functional forms utilized for pair interactions in the original EAM,[56] and are given by:

$$\phi_{\mathrm{OO}} = a_{\mathrm{OO}} e^{-4 r_0 r_{\mathrm{OO}}}, \qquad (33)$$

$$\phi_{\mathrm{OH}} = 2 \left[a_{\mathrm{OH}} r_{\mathrm{OH}} + b_{\mathrm{OH}} e^{-r_0 r_{\mathrm{OH}}} + \frac{c_{\mathrm{OH}}}{r_{\mathrm{OH}}^{24}} \right] \mathcal{S}(r_{\mathrm{OH}} - r_{cut}), \qquad (34)$$

and

$$\phi_{\mathrm{HH}} = 2 a_{\mathrm{HH}} e^{-2 r_0 r_{\mathrm{HH}}} \mathcal{S}(r_{\mathrm{HH}} - H_{cut}). \qquad (35)$$

In these expressions, $r_0 = 1$ has dimensions of $\mathrm{\AA}^{-1}$, and $\mathcal{S}(t)$ is the switching function defined in Eq. (18). ϕ_{HH} and ϕ_{OO} are purely repulsive. They damp to zero beyond their respective cutoffs r_{cut} and H_{cut} (the latter is specified in Table V). For consistency, r_{cut} is taken to be the same value as used above for determining whether

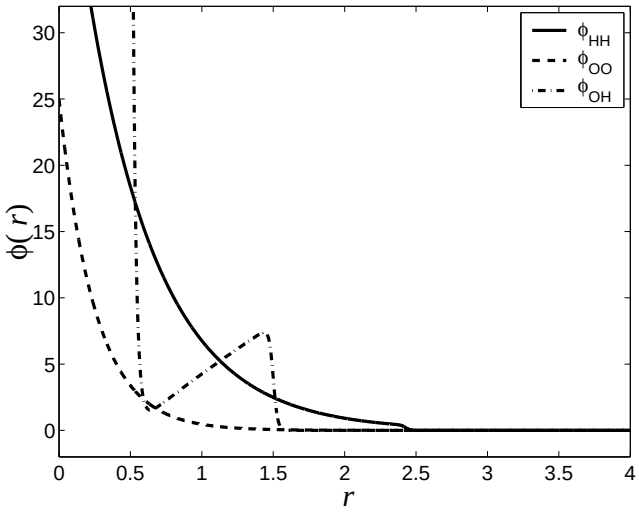

FIG. 4: Pair interaction potentials (in eV) as a function of internuclear separation r (in Å), for H-H, O-O, and O-H.

an H atom belongs to a particular cluster. This prevents non-coulombic H-H and O-H interactions between atoms in different clusters, for geometries near equilibrium. Note that $\phi_{\rm OH}$ has been designed to be very repulsive at small O-H separations by including an $r_{\rm OH}^{-24}$ term; this prevents the appearance of unphysical energy minima. The pair potentials are plotted in Fig. 4. The unusual "coat-hanger" shape of $\phi_{\rm OH}$ is a consequence of the fact that the pair potentials are parameterized in conjunction with the electrostatic term ϕ_{ij}, as part of an overall fit (*cf.* Eqs. (31) and (32)). The particular shape prevents O–H interactions between neighboring clusters.

The parameterization of the embedding functions and non-coulombic interactions was carried out with respect to a set of reference energies. We chose the symmetric mode of the monomer for three different bond angles (105.9, 100, and 110°) and the equilibrium geometry of the dimer as our reference configurations. Energies at each geometric configuration were obtained by subtracting the isolated atom energies from the total energy obtained via *ab initio* UHF 6-31G** calculations using `GAMESS`. The energy of the isolated oxygen computed using this basis set was −74.7839 hartrees and that of the isolated hydrogen atom equaled −0.5 hartrees. $A_{\rm O}^d$ and $A_{\rm H}^d$ are constants given in Table V.

For an oxygen atom O in a cluster with N hydrogens ($N \geq 2$),

$$A_{\rm O} \;=\; -A_{\rm EO} \sum_{j=1}^{N} \sum_{k=j+1}^{N} \sin^2(\theta_{j{\rm O}k}) \times \exp\Big[-\frac{1}{2} r_0^2 \left(r_{{\rm O}j} - r_{{\rm O}k}\right)^2 \sin^2(\theta_{j{\rm O}k}) \Big], \quad (36)$$

where j and k represent the j^{th} and k^{th} hydrogens in the cluster, and $A_{\rm EO}$ is defined in Table V. If $N = 1$, we set $A_O = 2A_{\rm EO}$.

If a hydrogen atom p that belongs to a cluster containing the oxygen atom s is involved in hydrogen bonding with $N_{\rm OH}$ oxygens of $N_{\rm OH}$ different neighboring clusters, then

$$A_{\rm H} = A_{\rm EH} \left[1 + \eta \sum_{u=1}^{N_{\rm OH}} \left(\Big[\exp\Big(-2[1+\cos(\theta_{ups})]^2 \Big) \Big] \Big[1 - \tanh\left(\frac{r_{up} - r_{hs}}{t_2} \right) \Big] \right) \right], \quad (37)$$

where u is the index corresponding to the neighboring clusters, θ_{ups} is the angle between $\overrightarrow{pu}$ and $\overrightarrow{ps}$, and η, r_{hs}, t_2 and A_{EH} are defined in Table V. Here we have again invoked a switching function in order to avoid energy discontinuities. If a given hydrogen atom is not involved in hydrogen bonding, then $A_H = A_{\rm EH}$.

Figure 5 depicts the actual (UHF calculations) and model-predicted variation in energy of the water monomer as a function of OH distance for the symmetric mode at the equilibrium angle. Table VI gives a comparison of the monomer properties as predicted by our potential, UHF calculations, and experiment. We used a modified[93] BFGS routine with analytic evaluation of gradients to determine the minimum energy (equilibrium) geometry.

It is evident from the table as well as from Fig. 5 that the energetics and the minimum energy structure of the monomer are well reproduced. However, the dipole moment of the monomer as predicted by our potential is significantly lower than experiment. Of course, there is no physical reason to expect the Löwdin charges to reproduce the dipole moments computed as proper expectation values. Indeed, if we choose instead a definition of the atomic charge based on a physical observable (the dipole moment),[94] we obtain the following effective local (static) and nonlocal (dynamic) contributions to the atomic charge on oxygen in the monomer: $Z^*_{\rm loc} = \mu(r)/r|_{\rm eq} = -0.541$ and $Z^*_{\rm nl} = r\,\partial Z^*_{\rm loc}(r)/\partial r|_{\rm eq} = -0.229$, where r refers in this case to the OH distance, and the derivative is evaluated for the symmetric stretch

TABLE V: Energy parameters. $a_{\rm OO}$, $a_{\rm OH}$, $a_{\rm HH}$, and $b_{\rm OH}$ in eV; $c_{\rm OH}$ in units eV $\cdot$ Å^{24}; $A_{\rm EO}$, $A^d_{\rm O}$, $A_{\rm EH}$, and $A^d_{\rm H}$ in eV/e; H_{cut}, r_{hs}, and t_2 in Å; η is dimensionless.

$a_{\rm OO}$	$a_{\rm OH}$	$a_{\rm HH}$	$b_{\rm OH}$	$c_{\rm OH}$	$A_{\rm EO}$	$A^d_{\rm O}$	$A_{\rm EH}$	$A^d_{\rm H}$	H_{cut}	r_{hs}	t_2	η
25.0	3.0111	25.0	−2.4053	2.5×10^{-6}	−11.429	0.0	4.7621	−0.5	2.43	2.1	0.1	0.0505

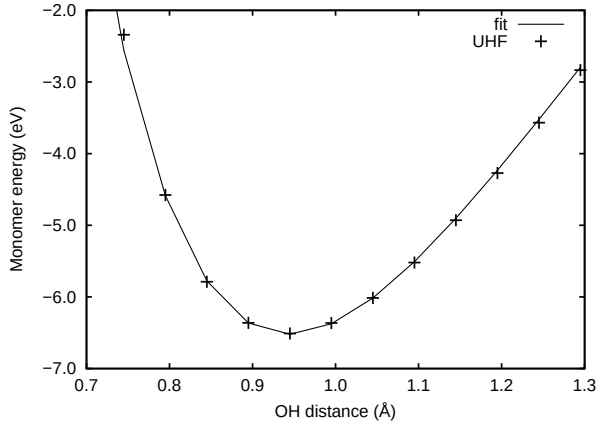

FIG. 5: UHF and predicted energies for a water monomer for the symmetric mode at the equilibrium angle.

TABLE VI: Monomer equilibrium properties.

	Predicted[a]	UHF[a]	Expt.
R_{eq} (Å)	0.9431	0.9431	0.957[b]
θ_{eq} (deg)	105.47	105.99	104.52[b]
μ (D)	1.23	2.19	1.86[c]
E_{eq} (eV)	−6.51	−6.52	—

[a]Present work.
[b]Ref. 88.
[c]Ref. 89.

mode at fixed, computed equilibrium angle. The total Born effective charge $Z^* = -0.770$ is given by the sum of the local and nonlocal contributions. This value can be compared with $Z_{\rm Löwdin} = -0.444$. Similar results would be expected for the dimer, where the Löwdin value for the dipole moment is in fortuitously good agreement with experiment.

Table VII contains information about the equilibrium properties of the water dimer (*i.e.*, its minimum energy configuration properties), with the geometry defined in Fig. 6. The binding energy U is obtained by subtracting the two monomer equilibrium energies from the total energy. For comparison, we also include the relevant experimental and UHF results. Once again, we are able to reproduce the dimer properties reasonably well with our potential.

At this stage it is important to recall that the parameters in our final energy model have been determined so as to represent the energetics of select geometries of the water monomer, and to yield the correct minimum energy

TABLE VII: Equilibrium properties of the water dimer. All distances in Å; angles in degrees; binding energy U in kcal/mol; μ in D.

	Predicted[a]	UHF[a]	Expt.[b]
$r_{\rm O_1H_1}$	0.941	0.948	—
$r_{\rm O_1H_2}$	0.952	0.942	—
$r_{\rm O_2H_1}$	1.937	2.038	—
$r_{\rm O_2H_{4/3}}$	0.943	0.944	—
$r_{\rm O_1O_2}$	2.886	2.98	2.952
$\angle_{\rm H_1O_1H_2}$	105.44	105.91	—
$\angle_{\rm H_3O_2H_4}$	105.37	106.31	—
$\angle_{\rm O_1H_2O_2}$	177.3	179.27	174.0
φ	1.8	−0.5	0.0 ± 6.0
ψ	60.9	56.7	58.0 ± 6.0
U	−5.860	−5.505	-5.40 ± 0.7
μ	2.30	2.60	2.64

[a]Present work.
[b]Refs. 90,91.

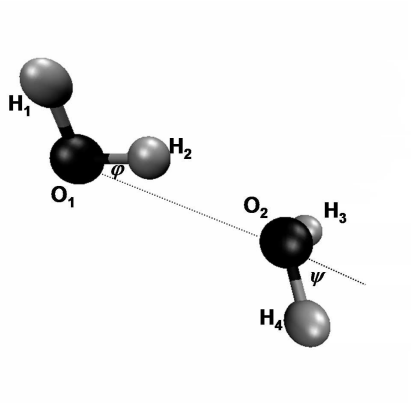

FIG. 6: Structural parameters defining the optimized water dimer structure.

structure of the water dimer. No energetic information for the remaining two model clusters used in the charge parameterization step—H_3O^+ and OH^-—was included in this *energy* parameterization process. Consequently, we should not expect the model in its current form to be able to accurately predict the energetics of ionic molecular species. We therefore focus on assessing the predictions of the potential for the structure and energetics of small neutral water clusters. These results are summarized in the following section.

IV. RESULTS

In developing a model capable of accurately describing water polymorphs, a basic but important requirement is the ability to predict the correct structure and binding energies of neutral vapor-phase water clusters.[95] There have been numerous computational[26,38,45,86,96,97,98,99,100,101,102] and experimental studies[105,106,107,108,109,110,111,112,114] examining various water clusters. It has been shown that small neutral water clusters have 2D cyclic structures, where each molecule serves as both an acceptor and a donor, while the larger clusters have 3D structures. This crossover is seen for the water hexamer and larger clusters, where the 3D structures are energetically favored. Some of the popular water potentials (MCDHO, TIP5P, TIP4P, POL5, Dang and Chang (DC)) have been used to study small water clusters with varying degrees of success. In the following, we compare our results with these potentials, as well as experiments and quantum calculations. We pay particular attention to the different structures of the hexamer.

A. Small water clusters: trimer-pentamer

Early spectroscopic studies[114] predicted the open chain conformation to be the most stable structure for the trimer. Subsequent work has suggested otherwise,[100,106] and the cyclic trimer with C_1 symmetry has been shown to be the more stable structure. Using the modified BFGS routine to perform the energy minimization, we found the ring structure to be slightly more stable than the open chain conformation with the difference in energy being 0.861 kcal/mol (this lies within the margin of error for our potential fit, 0.02 eV/molecule $\times$ 3 = 1.38 kcal/mol.) Next, we obtained the energies and optimized geometries of the predicted ground-state structure of the tetramer and pentamer. The S_4 cyclic tetramer structure has been shown to be most energetically favored for the water tetramer.[112] In this structure (Fig. 7(c)), there are alternating hydrogen atoms above and below the plane of the tetramer ring. A puckered cyclic ring (Fig. 7(d)) has been predicted to be the most stable pentamer structure by both *ab initio* calculations[100] and experiment.[108]

Table VIII gives the properties of the three clusters; for comparison, along the lines of Stern *et al.*,[45] we present results of select potentials along with *ab initio* calculations and experiment. The notation $\langle \cdots \rangle$ in Tables VIII–XII reflects the fact that all quoted distances are averaged over the cluster structure. Though our model predicts the correct structure and energetics, the net dipole moment μ is once again smaller than that computed via other models as well as experiment, as expected based on our previous discussion. Scaling μ by a factor equal to the ratio of the experimental monomer dipole moment and our model's monomer dipole moment (μ_{norm}= 0.6613) yields values that are more realistic; these are the values reported in Table VIII.

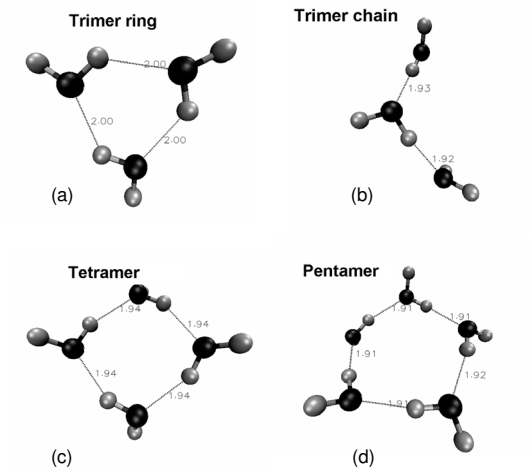

FIG. 7: Equilibrium geometries of H_2O_n, n=3-5; interatomic distances in Å.

B. Water hexamer

For the water hexamer, it has now been established that there are a number of different local minima structures that are energetically very comparable. IR spectroscopic experiments on gas-phase clusters by Paul *et al.*[116] and Liu *et al.*[109,110] indicate that the caged hexamer structure is the most stable, while *ab initio* calculations have revealed that the cage, prism and book structures are almost degenerate, with the stability sequence depending on the inclusion of zero-point energy differences.[117,118,119,120,121,122,123] Further, Tissandier *et al.*[115] have used a topological enumeration technique in conjunction with semi-empirical PM3 methods to predict the global minimum energy structures. Here we examine the cyclic, cage, prism, chair and book structures; the results are provided in Tables IX and X. The prism, book and the cage structures are the most stable and are energetically nearly degenerate, while the cyclic and chair are clearly metastable structures at 0 K. The computed dipole moment μ has been scaled by μ_{norm}. Fig. 8 shows the various water hexamers as obtained from our model. The results clearly indicate that our model is capable of describing the experimentally determined structures and relative energetics of the water hexamers.

C. Beyond the Hexamer

The experimental energetics and the structures of water clusters with six or fewer molecules have been well documented.[88,89,90,91,105,106,107,108,109,110,111,112] This is not true for larger water clusters ($n \geq 10$), and informa-

TABLE VIII: Equilibrium properties of water clusters (n=3–5). All distances in Å, angles in degrees, energies in kcal/mol, charge in e, and dipole moment μ in debye (D). 6-31G** HF energies are given in parentheses along with select *ab initio* values.

	Predicted	POL5/TZ[a]	POL5/QZ[a]	TIP4P/FQ[b]	TIP5P[c]	MCDHO[d]	*ab initio*	Expt.
Trimer– Cyclic								
U	−13.743	−13.416	−13.453	−12.576	−14.992	−13.982	−15.9[e] (−17.10)	
$\langle r_{\rm OO}\rangle$	2.712	2.901	2.893	2.912	2.770	2.911	2.782[e]	2.960[h]
μ	0.673	1.205	1.205	0.417	1.074	1.114	1.071[f]	
$\langle \angle_{\rm HOH}\rangle$	105.26							
$\langle r_{\rm OH}\rangle$	0.949							
$\langle q_{\rm H}\rangle$	0.221							
Tetramer– Cyclic								
U	−27.308	−25.529	−25.665	−23.641	−28.431	−27.581	−23.8[g] (−29.10)	
$\langle r_{\rm OO}\rangle$	2.826	2.769	2.759	2.809	2.673	2.806	2.743[g]	2.79[h]
μ	0.015	0.000	0.000	0.000	0.000	0.024	0.000[f]	
$\langle \angle_{\rm HOH}\rangle$	105.27							
$\langle r_{\rm OH}\rangle$	0.948							
$\langle q_{\rm H}\rangle$	0.220							
Pentamer– Cyclic								
U	−36.027	−34.111	−34.427	−32.954	−38.122	−35.229	−33.34[g] (−37.70)	
$\langle r_{\rm OO}\rangle$	2.850	2.742	2.726	2.773	2.657	2.753	2.867[g]	2.760[h]
μ	0.634	1.190	1.191	0.401	1.219	0.992	0.927[f]	
$\langle \angle_{\rm HOH}\rangle$	105.26							
$\langle r_{\rm OH}\rangle$	0.948							
$\langle q_{\rm H}\rangle$	0.220							

[a]Ref. 45.
[b]Refs. 26,45.
[c]Ref. 37.
[d]Ref. 38.
[e]Ref. 101.
[f]Refs. 103,104.
[g]Ref. 100.
[h]Refs. 105,106 (trimer); 111,112 (tetramer); 107,108 (pentamer).

tion about such clusters is available mainly via classical potentials and quantum calculations. Hence we compare our results only with other computational studies.[86,96,97] Maheshwary *et al.*[86] have examined the structure and stability of water clusters (up to twenty-molecule clusters) using Hartree Fock as well as DFT (B3LYP) calculations with 6-31G** and 6-31++G** basis sets; calculations using TIP4P[97] and TIP5P[96] potentials have also been performed for these clusters.

The experimentally-determined[124] and theoretically predicted[86] stable heptamer conformer is a cuboid structure with a missing corner, labeled Heptamer (a) in Fig. 9. This is also the lowest energy geometry as predicted by our potential, with an unscaled dipole moment of 1.20 D. In addition, we observe another structure (Heptamer (b) in Fig. 9) to be approximately 1 kcal/mol higher in energy. This structure has a high dipole moment (3.94 D), and nine hydrogen bonds, in contrast to the ten found in the more stable conformer. Note that the dipole moments reported in Table XI for the large clusters are as obtained and have not been rescaled, since no experimental data is available for comparison. (We also would expect the deviation between theory and experiment resulting from our specific choice of atom-in-molecule charge definition to "wash out" for the larger clusters.) The same ordering in the energies and dipole moments is seen in the work of Maheshwary *et al.*[86]

The most stable state of the water octamer in our work is cubic with D_{2d} symmetry. The next most stable octamer structure is another cubic structure with $S4$ symmetry. We observe a difference of almost 1.4 kcal/mol in the relative energies of the two structures; Maheshwary *et al.*[86] predict the two structures to be nearly isoenergetic. The dipole moment is zero for both structures, with each structure characterized by twelve hydrogen bonds. These structures are shown in Fig. 9.

The global minimum water nanomer structure can be described in terms of a pentamer and a tetramer ring con-

TABLE IX: Equilibrium properties of water hexamers I. All distances in Å, angles in degrees, energy in kcal/mol, charge in e, and dipole moment μ in D. 6-31G** HF energies are given in parentheses along with select *ab initio* values.

	Predicted	POL5/TZ[a]	POL5/QZ[a]	TIP4P/FQ[b]	TIP5P[c]	MCDHO[d]	DC[e]	*ab initio*	Expt.
Hexamer– Cage									
U	−46.497	−41.783	−39.297	−45.388	−45.388	−43.690	−40.76	−45.03[f] (−48.60)	
$\langle r_{OO}\rangle$	2.801	2.783	2.755	2.863	2.746	2.888		2.807[f]	2.820[h]
μ	2.120	2.442	2.454	1.788	2.178	2.034		2.05[g]	1.904[h]
$\langle \angle_{HOH}\rangle$	105.14								
$\langle r_{OH}\rangle$	0.950								
$\langle q_H\rangle$	0.220								
Hexamer– Book									
U	−46.492	−42.464	−42.771	−40.152	−46.680	−43.977	−40.38	−44.74[f]	
$\langle r_{OO}\rangle$	2.788	2.777	2.777	2.815	2.688	2.809		2.766[f]	
μ	2.410	2.449	2.430	2.006	2.445				
$\langle \angle_{HOH}\rangle$	105.22								
$\langle r_{OH}\rangle$	0.949								
$\langle q_H\rangle$	0.220								
Hexamer– Prism									
U	−46.465	−41.847	−42.135	−39.304	−45.805	−44.192	−40.97	−45.12[f] (−49.60)	
$\langle r_{OO}\rangle$	2.757	2.792	2.782	2.819	2.773	2.892		2.840[f]	
μ	2.974	2.905	2.931	3.254	2.692	2.627		2.701[g]	
$\langle \angle_{HOH}\rangle$	104.85								
$\langle r_{OH}\rangle$	0.951								
$\langle q_H\rangle$	0.219								

[a]Ref. 45.
[b]Ref. 26,45.
[c]Ref. 37.
[d]Ref. 38.
[e]Ref. 52.
[f]Ref. 99.
[g]Refs. 103,104.
[h]Refs. 109,110.

nected by hydrogen bonds (Nanomer (a) in Fig. 9). This structure is seen by experimental studies of Buck *et al.*[125] as well as computational studies by Maheshwary *et al.*[86] and Dang and Chang,[52] and is characterized by thirteen hydrogen bonds. Our potential also predicts this structure to be the most stable. Another stationary point on the nanomer energy surface is the structure Nanomer (b) as shown in Fig. 9. This structure contains 13 hydrogen bonds, and can be described as a octamer cube plus a monomer coordinated to a corner of the cube via a hydrogen bond.

Locating the global energy minimum for larger clusters ($n \geq 10$) is a difficult task since the flat potential energy surface gives rise to many possible geometries with comparable energies. We have therefore used the geometries predicted by Maheshwary *et al.*,[86] TIP5P,[96] and TIP4P[97] (available online at the Cambridge cluster database website[113]) as starting configurations for our energy minimization calculations. The energies of our resulting energy-minimized structures for $n = 10 - 20$ (Table XII), agree reasonably well with the calculations of Maheshwary *et al.* Rather than providing the geometries of all the above clusters, we have listed their important properties in Table XII; the table also indicates the initial structure that yields the minimum energy geometry when we perform our minimization.

A summary comparison of our model-predicted results with the *ab initio* calculations of Maheshwary *et al.* is given in Fig. 10. Some deviations from the *ab initio* results occur at $n = 3$, 6, and 16. In particular, as shown in Table VIII, we underestimate the binding energy of the trimer, leading to the deviation in estimation of the incremental interaction energy at $n = 3$. Although the model is able to predict the correct ordering of the binding energies of the various hexamers and heptamer, it is unable to capture the small difference in incremental interaction energy between $n = 6$ and $n = 7$. However, we do largely reproduce the alternation in stability of the

TABLE X: Equilibrium properties of water cluster hexamers II. All distances in Å, angles in degrees, energy in kcal/mol, charge in e, and dipole moment μ in D. 6-31G** HF energies are given in parentheses along with select *ab initio* values. Footnotes as in Table IX.

	Predicted	POL5/TZ[a]	POL5/QZ[a]	TIP4P/FQ[b]	TIP5P[c]	MCDHO[d]	DC[e]	*ab initio*	Expt.
Hexamer– Chair									
U	−44.073								
$\langle r_{\rm OO}\rangle$	2.846								
μ	0.011								
$\langle \angle_{\rm HOH}\rangle$	105.25								
$\langle r_{\rm OH}\rangle$	0.948								
$\langle q_{\rm H}\rangle$	0.220								
Hexamer– Cyclic									
U	−43.919	−41.875	−42.224	−41.368	−47.309	−44.264	−39.34	−43.88[f]	
$\langle r_{OO}\rangle$	2.849	2.737	2.720	2.756	2.654	2.731		2.714[f]	2.756[g]
μ	0.150	0.017	0.003	0.000	0.000	0.134		0.000	
$\langle \angle_{HOH}\rangle$	105.25								
$\langle r_{OH}\rangle$	0.948								
$\langle q_{\rm H}\rangle$	0.220								

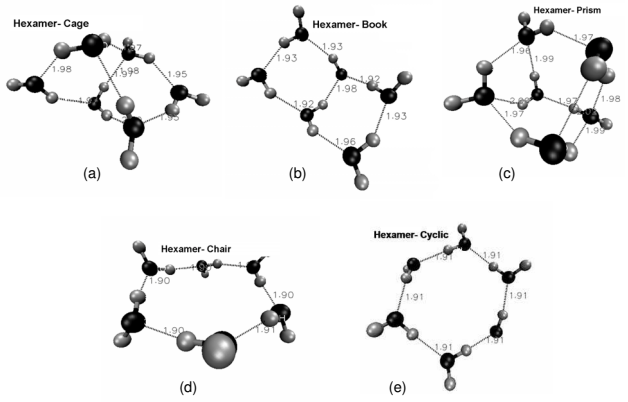

FIG. 8: Equilibrium geometries of water hexamers; interatomic distances in Å.

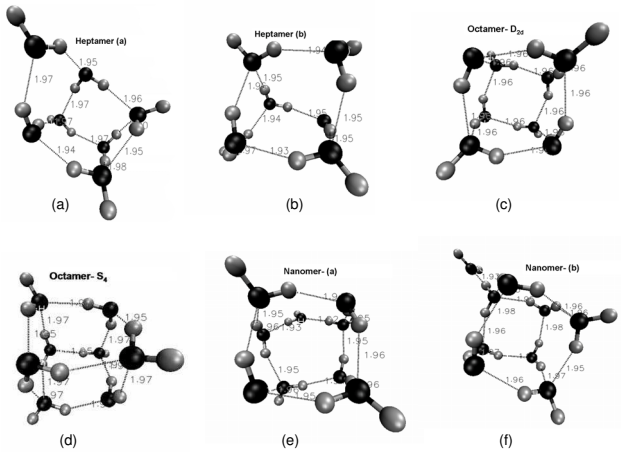

FIG. 9: Equilibrium geometries of H_2O_n, n=7-9; interatomic distances in Å.

cluster depending on whether n is odd or even—in particular, the enhanced stability of even n-mers relative to odd n-mers.

V. DISCUSSION AND CONCLUSIONS

We have presented a new dynamical CT-EAM potential for modeling water and its polymorphs at the atomic level. We have based our parameterization on *ab initio* data; in particular, atomic charge fluctuations have been modelled with reference to the local chemical environment, using Löwdin population analysis to represent atomic charges. Depending on its immediate coordination environment, each atom is assigned to a cluster, with this identification being crucial to our formulations. Cluster identification is effected via a radial cutoff, and total cluster charge is based on the size of the cluster and relative positions of neighboring clusters. This charge is in turn partitioned among the constituent atoms.

Our technique is sufficiently flexible to account for very different charge states of clusters and individual atoms. The radial cutoff chosen to define our clusters, $r_{cut} = 1.5$ Å, is significantly larger than the O−H equilibrium distance in the monomer and dimer ($\sim$ 0.95 Å.) Consequently, the model is easily capable of describing non-perturbative charge transfer.

We note that a number of important effects have been

TABLE XI: Equilibrium properties of water clusters for n=7-9. All distances in Å, angles in degrees, energy in kcal/mol, charge in e, and dipole moment μ in D.

	Predicted	TIP4P[a]	TIP5P[b]	*ab initio*[c]
Heptamer (a)				
U	−58.259	−58.271	−57.910	−60.53
$\langle r_{\rm OO}\rangle$	2.802	2.762	2.738	2.884
μ	1.20			1.35
$\langle \angle_{\rm HOH}\rangle$	105.09			106.26
$\langle r_{\rm OH}\rangle$	0.951			0.950
$\langle q_{\rm H}\rangle$	0.219			
Octamer D_{2d}				
U	−74.325	−73.090	−72.535	−76.01
$\langle r_{\rm OO}\rangle$	2.822	2.746	2.712	2.877
μ	0.00			0.00
$\langle \angle_{\rm HOH}\rangle$	105.13			106.482
$\langle r_{\rm OH}\rangle$	0.951			0.951
$\langle q_{\rm H}\rangle$	0.219			
Nanomer (a)				
U	−84.124	−82.401	−83.622	−85.05
$\langle r_{OO}\rangle$	2.842	2.741	2.696	2.869
μ	0.99			1.69
$\langle \angle_{\rm HOH}\rangle$	105.16			106.39
$\langle r_{\rm OH}\rangle$	0.950			0.950
$\langle q_{\rm H}\rangle$	0.219			

[a]Ref. 97.
[b]Ref. 96.
[c]Ref. 86.

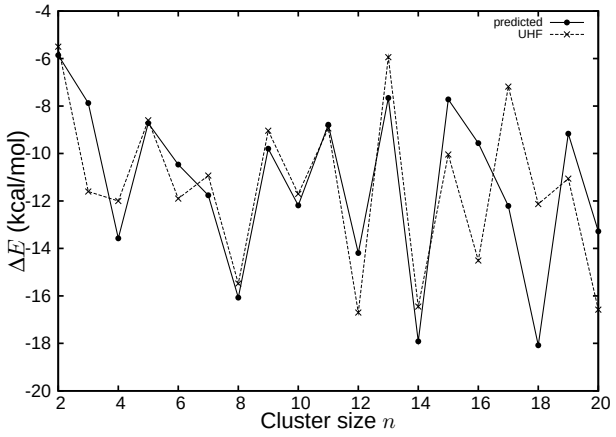

FIG. 10: Incremental interaction energies of water clusters, $\Delta E = E_{n+1} - E_n - E_1$, as a function of cluster size n. Note that $\Delta E = U_{n+1} - U_n$, where U_n is the binding energy for a cluster of size n. UHF results from Ref. [86].

omitted in this initial implementation. This was done in order to focus attention on the physics of the charge-transfer EAM model framework itself, rather than the refinement of a model water potential *per se.* For example, the current parameterization does not yet impose the correct asymptotic dissociation behavior on cluster subsystems, which we have argued is critical to a proper description of reactive dynamics.[69,71] A related issue concerns the omission of several ionic species, believed to be important in defining the hydrogen network in water, from our parameterizations: these include the Zundel ($H_5O_2^+$) and Eigen ($H_9O_4^+$) cations.[22] A final important simplification concerns the use of atom-in-molecule charges as proxies for the shape function modeling of the AIM charge-density distributions. It is clear that further work taking account of these various factors will be necessary in order to successfully study complex kinetic processes such as those involved in ion solvation, enzyme catalysis, and proton transport. This work is presently underway. Additionally, it should be noted that our approach does not incorporate a quantum mechanical treatment of the actual electron or proton transfer processes.[126]

Notwithstanding the simplicity of this initial model, in tests on small water clusters, our results agree very well with experimental and *ab initio* data. Importantly, our model captures the transition from planar ring pentamer structures to three-dimensional complex hexamer structures, an essential structural test for any successful water potential. In this context, it is worth noting that an environment dependent dynamic charge potential motivated by the present work has also been developed recently for silica. This potential successfully matches *ab initio* results in its ability to predict the ground-state energy, geometry and failure mechanisms of silica clusters.[127]

More generally, this work represents a successful application of many-body embedded atom concepts to the modeling of a highly polarizable *molecular* system, and thus a significant departure from traditional approaches to developing water potentials. It is remarkable that even this relatively simple implementation of CT-EAM reproduces cluster structures and energetics consistent with the best previous potentials, while providing a theoretical roadmap for implementing true charge-transfer dynamics. This ability of an embedded-atom approach—originally designed for describing many-body effects in bulk *fcc* metals—to model the structure of a molecular system can be understood as a direct consequence the CT-EAM framework's underlying density functional construction. DFT, with its emphasis on electron densities as the fundamental variables of the theory, acts as a multiscale mechanism for incorporating quantum mechanical bonding effects and excitations within a nominally classical potential.

We believe that the unique combination of features described here will ultimately enable CT-EAM potentials to successfully capture many-body and electrostatic effects, in both static and dynamic contexts, for a wide variety of biophysical and materials systems, including

TABLE XII: Predicted equilibrium cluster-averaged properties of water clusters for $n \geq 10$. All distances in Å, angles in degrees, energy in kcal/mol, charge in e, and dipole moment μ in D. "Geometry" refers to the starting geometry for the energy minimization, as described in the text.

n	U	$\langle r_{\mathrm{OO}} \rangle$	μ	$\langle \angle_{\mathrm{HOH}} \rangle$	$\langle r_{\mathrm{OH}} \rangle$	$\langle q_{\mathrm{H}} \rangle$	Geometry
10	−96.311	2.841	1.81	105.12	0.951	0.219	TIP5P
11	−105.098	2.849	2.54	104.97	0.952	0.219	TIP5P
12	−119.291	2.828	0.00	104.87	0.953	0.219	Ref. [86]
13	−126.951	2.835	1.65	105.11	0.951	0.219	TIP4P
14	−144.868	2.835	1.86	105.01	0.952	0.218	TIP4P
15	−152.589	2.850	1.98	105.12	0.951	0.218	TIP5P
16	−162.153	2.829	0.00	104.73	0.954	0.219	TIP4P
17	−174.362	2.848	3.03	105.02	0.952	0.219	TIP5P
18	−192.442	2.836	1.85	104.93	0.953	0.218	TIP4P
19	−201.608	2.842	2.97	105.03	0.952	0.218	TIP5P
20	−214.889	2.833	0.17	104.93	0.953	0.218	TIP4P

nanoscale systems possessing mixed molecular and bulk features. Future applications will include studies of the crystalline polymorphs of water and the thermodynamic and structural properties of the liquid, as well as investigations of dynamical processes such as ion solvation and proton transport.

VI. ACKNOWLEDGEMENTS

We thank Dr. Keith Runge (University of Florida) for many useful insights, Dr. Andy Pineda (University of New Mexico) for assistance with `GAMESS`, and the UNM Center for High Performance Computing for computational resources. This work was supported by NSF Grant No. CHE-0304710. S.R.A. gratefully acknowledges support from NSF Grant No. DMR-9520371 during the early stages of this research. The work of S.M.V. was performed at Los Alamos National Laboratory under the auspices of the U.S. Department of Energy, under contract No. DE-AC52-06NA25396. One of the authors (K.M.) would like to thank Prof. Sam Trickey and the University of Florida Quantum Theory Project for postdoctoral support under NSF ITR award DMR-0325553, where portions of this work were completed.

* Electronic address: susie@sapphire.phys.unm.edu

[1] B. R. Brooks, R. E. Bruccoleri, B. D. Olafson, D. J. States, S. Swaminathan, and M. Karplus, J. Comp. Chem. **4**, 187 (1983).

[2] A. C. T. van Duin, S. Dasgupta, F. Lorant, and W. A. Goddard III, J. Phys. Chem. A **105**, 9396 (2001); Q. Zhang, T. Çağin, A. van Duin, W. A. Goddard III, Y. Qi, and L. G. Hector, Jr., Phys. Rev. B **69**, 045423 (2004).

[3] L. Huang and J. Kieffer, J. Chem. Phys. **118**, 1487 (2003); A. Alavi, L. J. Alvarez, S. R. Elliott, and I. R. McDonald, Phil. Mag. B **65**, 489 (1992).

[4] E. Demiralp, T. Cagin, and W.A. Goddard III, Phys. Rev. Lett. **82**, 1708 (1999); B. S. Thomas, N. A. Marks, and B. D. Begg, Phys. Rev. B **69**, 144122 (2004).

[5] F. H. Streitz and J. W. Mintmire, Phys. Rev. B **50**, 11996 (1994).

[6] F. H. Streitz and J. W. Mintmire, Thin Solid Films **253**, 179 (1994); F. H. Streitz and J. W. Mintmire, Langmuir **12**, 4605 (1996).

[7] M. S. Daw and M. I. Baskes, Phys. Rev. Lett. **50**, 1285 (1983).

[8] M. S. Daw and M. I. Baskes, Phys. Rev. B **29**, 6443 (1984).

[9] M. S. Daw, S. M. Foiles, and M. I. Baskes, Mater. Sci. Rep. **9**, 251 (1993).

[10] M. I. Baskes, Phys. Rev. Lett. **59**, 2666 (1987); M. I. Baskes, J. S. Nelson, and A. F. Wright, Phys. Rev. B **40**, 6085 (1989); M. I. Baskes, Phys. Rev. B **46**, 2727 (1992); M. I. Baskes, Mater. Chem. Phys. **50**, 152 (1997).

[11] J. C. Slater and G. F. Koster, Phys. Rev. **94**, 1498 (1954); A. P. Sutton, M. W. Finnis, D. G. Pettifor and Y. Ohta, J. Phys. C: Solid State Phys. **21**, 35 (1988); D. A. Papaconstantopoulos and M. J. Mehl, J. Phys. Cond. Matt. **15**, R413 (2003).

[12] M. Elstner, D. Porezag, G. Jungnickel, J. Elsner, M. Haugk, T. Frauenheim, S. Suhai, and G. Seifert, Phys. Rev. B **58**, 7260 (1998); Q. Cui, M. Elstner, E. Kaxiras, T. Frauenheim, and M. Karplus, J. Phys. Chem. B **105**, 569 (2001).

[13] F. O. Ellison, J. Am. Chem. Soc. **85**, 3540 (1963); J. C. Tully, J. Chem. Phys. **58**, 1396 (1973); J. C. Tully, in: G. A. Segal, Ed. *Semiempirical Methods of Electronic Structure Calculation* (Plenum, New York, 1977), p. 173.

[14] A. Warshel and A. Bromberg, J. Chem. Phys. **52**, 1262 (1970); A. Warshel and R. M. Wiess, J. Am. Chem. Soc. **102**, 6218 (1980); J. Åqvist and A. Warshel, Chem. Rev.

93, 2523 (1993).
[15] T. J. F. Day, A. V. Soudackov, M. Čuma, U. W. Schmitt, and G. A. Voth, J. Chem. Phys. **117**, 5839 (2002).
[16] A. Warshel and M. Levitt, J. Mol. Biol. **103**, 227 (1976); U. C. Singh and P. A. Kollman, J. Comput. Chem. **7**, 718 (1986); M. J. Field, P. A. Bash, and M. Karplus, J. Comp. Chem. **11**, 700 (1990).
[17] S. M. Valone and S. R. Atlas, Phil. Mag. **86**, 2683 (2006).
[18] S. R. Atlas and S. M. Valone, Density functional theory of the embedded-atom method: Multiscale dynamical potentials with charge transfer (to be submitted).
[19] P. Hohenberg and W. Kohn, Phys. Rev. **136**, B864 (1964).
[20] W. Kohn and L. J. Sham, Phys. Rev. **140**, A1133 (1965).
[21] A. J. Stone, Science **315**, 1228 (2007).
[22] U. W. Schmitt and G. A. Voth, J. Chem. Phys. **111**, 9361 (1999).
[23] G. A. Secco, J. Chem. Phys. **23**, 1734 (1955).
[24] O. Dutuit, A. Tabache-Fouhaile, I. Nenner, H. Frohlich, and P. M. Guyon, J. Chem. Phys. **83**, 584 (1985).
[25] B. L. Henson, J. Phys. D **11**, 1405 (1978).
[26] S. W. Rick, S. J. Stuart, and B. J. Berne, J. Chem. Phys. **101**, 6141 (1994).
[27] A. E. Lefohn, M. Ovchinnikov, and G. A. Voth, J. Phys. Chem B **105**, 6628 (2001); J. Jeon, A. Lefohn, and G. Voth, J. Chem. Phys. **118**, 7504 (2003).
[28] O. Mishima and H. E. Stanley, Nature **396**, 329 (1998).
[29] J. L. Finney, J. Mol. Liq. **90**, 303 (2001).
[30] B. Guillot, J. Mol. Liq. **101**, 219 (2002).
[31] F. N. Keutsch and R. J. Saykally, Proc. Natl. Acad. Sci. (USA) **98**, 10533 (2001).
[32] F. H. Stillinger and A. Rahman, J. Chem. Phys. **60**, 1545 (1974).
[33] H. J. C. Berendsen, J. P. M. Postma, W. F. van Gunsteren, and J. Hermans, in *Intermolecular Forces,* edited by B. Pullman (Reidel, Dordrecht, 1981), p. 331.
[34] H. J. C. Berendsen, J. R. Grigera, and T. P. Straatsma, J. Phys. Chem. **91**, 6269 (1987).
[35] W. L. Jorgensen, J. Chandrasekhar, J. D. Madura, R. W. Impey, and M. L. Klein, J. Chem. Phys. **79**, 926 (1983).
[36] W. L. Jorgensen and J. D. Madura, Mol. Phys. **56**, 1381 (1985).
[37] M. W. Mahoney and W. L. Jorgensen, J. Chem. Phys. **112**, 8910 (2000).
[38] H. Saint-Martin, J. Hernandez-Cobos, M. I. Bernal-Uruchurtu, and I. Ortega-Blake, J. Chem. Phys. **113**, 10899 (2000).
[39] G. C. Groenenboom, E. M. Mas, R. Bukowski, K. Szalewicz, P. E. S. Wormer, and A. van der Avoird, Phys. Rev. Lett. **84**, 4072 (2000); E. M. Mas, R. Bukowski, K. Szalewicz, G. C. Groenenboom, P. E. S. Wormer, and A. van der Avoird, J. Chem. Phys. **113** 6687 (2000); R. Bukowski, K. Szalawicz, G. Groenenboom, and A. van der Avoird, J. Chem. Phys. **125**, 044301 (2006).
[40] G. Corongju and E. Clementi, J. Chem. Phys. **97**, 2030 (1992).
[41] U. Neisar, G. Corongju, E. Clementi, G. R. Kneller, and D. K. Battacharya, J. Phys. Chem. **94**, 7949 (1990).
[42] O. Matsuoka, E. Clementi, and M. Yoshimine, J. Chem. Phys. **64**, 1351 (1976).
[43] A. Wallqvist, P. Ahlström, G. Karlström, J. Phys. Chem. **94**, 1649 (1990).
[44] R. Bukowski, K. Szalewicz, G. C. Groenenboom, and A. van der Avoird, Science **315**, 1249 (2007).
[45] H. A. Stern, F. Rittner, B. J. Berne, and R. A. Freisner, J. Chem. Phys. **115**, 2237 (2001).
[46] R. Polák, I. Paidarová, and P. J. Kuntz, J. Chem. Phys. **82**, 2352 (1985); **87**, 2863 (1987); R. Polák and P. J. Kuntz, Mol. Phys. **63**, 865 (1988); A. J. C. Varandas, J. Chem. Phys. **105**, 3524 (1996); A. J. C. Varandas, J. Chem. Phys. **107**, 867 (1997); A. J. C. Varandas, A. I. Voronin, and P. J. S. B. Caridade, J. Chem. Phys. **108**, 7623 (1998).
[47] J. W. Halley, J. R. Rustad, and A. Rahman, J. Chem. Phys. **98**, 4110 (1993).
[48] R. L. Corrales, J. Chem. Phys. **110**, 9071 (1999).
[49] T. M. Truskett and K. A. Dill, Biophys. Chem. **105**, 449 (2003).
[50] S. B. Zhu and G. W. Robinson, Proc. Int. Conf. Supercomp. **II**, 189 (1989).
[51] S.-B. Zhu, S. Singh, and G. W. Robinson, J. Chem. Phys. **95**, 2791 (1991).
[52] L. X. Dang and T-M. Chang, J. Chem. Phys. **106**, 8149 (1997).
[53] C. Millot, J.-C. Soetens, M. T. C. Martins Costa, M. P. Hodges, and A. J. Stone, J. Phys. Chem. A **102**, 754 (1998).
[54] B. Guillot and Y. Guissani, J. Chem. Phys. **114**, 6720 (2001).
[55] C. J. Burnham, J. C. Li, S. S. Xantheas, and M. S. Leslie, J. Chem. Phys. **110**, 4566 (1999).
[56] S. M. Foiles, M. I. Baskes, and M. S. Daw, Phys. Rev. B **33**, 7983 (1986).
[57] F. J. Cherne, M. I. Baskes, and R. B. Schwarz, J. Non-Crystal. Sol. **317**, 45 (2003); Y. Mishin, A. Y. Lozovoi, and A. Alavi, Phys. Rev. B **67**, 014201 (2003).
[58] M. I. Baskes, K. Muralidharan, M. Stan, S. M. Valone, and F. J. Cherne, J. Metals **55**, 41 (2003).
[59] R. Ravelo and M.I. Baskes, Phys. Rev. Lett. **79**, 2482 (1997).
[60] S. M. Valone and V. Kapila, AIP Conf. Proc. **845**, 425 (2007).
[61] I. J. Robertson, V. Heine, and M. C. Payne, Phys. Rev. Lett. **70**, 1944 (1993).
[62] A. F. Voter, in: J. H. Westbrook and R. L. Fleischer, eds. *Intermetallic Compounds: Vol 1, Principles* (Wiley, New York, 1994).
[63] M. S. Daw, Phys. Rev. B **39**, 7441 (1989).
[64] E. M. Webb III and G. S. Grest, Phys. Rev. Lett. **86**, 2066 (2001).
[65] A. K. Rappé and W. A. Goddard, III, J. Phys. Chem. **95**, 3358 (1991).
[66] F. H. Streitz and J. W. Mintmire, Phys. Rev. B **60**, 773 (1999).
[67] T. Campbell, R. K. Kalia, A. Nakano, P. Vashishta, S. Ogata, and S. Rodgers, Phys. Rev. Lett. **82**, 4866 (1999); T. J. Campbell, G. Aral, S. Ogata, R. K. Kalia, A. Nakano, and P. Vashishta, Phys. Rev. B **71**, 205413 (2005).
[68] X. W. Zhou, H. N. Wadley, J.-S. Filhol and M. N. Neurock, Phys. Rev. B **69**, 2354 (2004).
[69] J. P. Perdew, R. G. Parr, M. Levy, and J. L. Balduz, Jr., Phys. Rev. Lett. **49**, 1691 (1982).
[70] J. P. Perdew, in: *Density Functional Methods in Physics*, NATO Advanced Science Institute Series, Vol. 123, edited by R. M. Dreizler and J. da Providência (Plenum Press, New York, 1984).
[71] S. M. Valone and S. R. Atlas, Phys. Rev. Lett. **97**, 256402 (2006).

[72] S. M. Valone and S. R. Atlas, J. Chem. Phys. **120**, 7262 (2004).

[73] S. M. Valone and S. R. Atlas, Fractional charge in diatomics-in-molecules Hamiltonians, *Abstracts of The 231st ACS National Meeting, Symposium in Honor of Robert G. Parr's 85th Birthday*, Atlanta, GA, March 26-30, 2006; S. Jindal and S. M. Valone (unpublished).

[74] See, e.g.: C. A. Mead and D. G. Truhlar, J. Chem. Phys. **70**, 2284 (1979); J. C. Tully, J. Chem. Phys. **93**, 1061 (1990); K. Ruedenberg and G. J. Atchity, J. Chem. Phys. **99**, 3799 (1993); D. F. Coker, in: P. P. Allen and D. J. Tildesley, eds. *Computer Simulation in Chemical Physics*, p. 315 (1993); D. R. Yarkony, J. Phys. Chem. A **105**, 6277 (2001); A. Toniolo, M. Ben-Nun, and T. J. Martinez, J. Phys. Chem. A **106**, 4679 (2002); A. Hellman, B. Razaznejad, and B. I. Lundqvist, J. Chem. Phys. **120**, 4593 (2004); A. W. Jasper, C. Zhu, S. Nangia, and D. G. Truhlar, Farad. Discuss. **127**, 1 (2004); A. W. Jasper and D. G. Truhlar, J. Chem. Phys. **122**, 044101 (2005).

[75] R. N. Dixon, D. W. Hwang, X. F. Yang, S. Harich, J. J. Lin, and X. Yang, Science **285**, 1249 (1999); D. Yarkony, Mol. Phys. **93**, 971 (1998).

[76] S. D. Kenny, D. Nguyen-Manh, H. Fujitani, and A. P. Sutton, Phil. Mag. Lett. **78**, 469 (1998).

[77] W. Moffitt, Proc. Roy. Soc. (London) **A210**, 245 (1951); Rept. Prog. Phys. **17**, 173 (1954).

[78] R. F. W. Bader, in *Atoms in Molecules: A Quantum Theory* (Oxford, New York, 1990).

[79] Y. Levy and J. N. Onuchic, Ann. Rev. Biophys. Biomol. Str. **35**, 389 (2005).

[80] S. B. Trickey, S. Yip, H-P. Chen, K. Runge, and P. A. Deeymier, J. Comp.-Aided Matls. Design **13**, 1 (2006); H-P. Chen, L-L. Wang, M-H. Du, C. Cao, Y-X. Wang, Y. He, K. Muralidharan, G. Greenlee, and A. Kolchin, J. Comp.-Aided Matls. Design **13**, 161 (2006).

[81] Q. Cui, Theor. Chem. Acc. **116**, 51 (2006).

[82] K. Takada, H. Sakurai, E. Takayama-Muromachi, F. Izumi, R. A. Dilanian, and T. Sasaki, Nature (London) **422**, 53 (2003); E. Dagotto, Science **309**, 257 (2005).

[83] M. W. Schmidt, K. K. Baldridge, J. A. Boatz, S. T. Elbert, M. S. Gordon, J. H. Jensen, S. Koseki, N. Matsunaga, K. A. Nguyen, S. J. Su, T L. Windus, M. Dupuis, J. A. Montgomery, J. Comput. Chem. **14**, 1347 (1993).

[84] The Löwdin atomic charge q_A for an atom A is defined as $q_A = Z_A - \sum_{\mu\in A}(S^{1/2}PS^{1/2})_{\mu\mu}$, where Z_A is the atomic charge, S is the matrix of basis function overlap integrals, and P is the density matrix expressed in terms of orbital basis-set expansion coefficients.[85]

[85] A. Szabo and N. S. Ostlund, *Modern Quantum Chemistry* (Dover, New York, 1996), p. 152.

[86] S. Maheshwary, N. Patel, N. Sathyamurthy, A. D. Kulkarni, and S. R. Gadre, J. Phys. Chem. A **105**, 10525 (2001).

[87] J. T. Su, X. Xu, and W. A. Goddard III, J. Phys. Chem. A **108**, 10518 (2004).

[88] W. S. Benedict, N. Gailar, and E. K. Plyler, J. Chem. Phys. **24**, 1139 (1956).

[89] A. S. Clough, Y. Beers, G. P. Klein, and L. S. Rothman, J. Chem. Phys. **59**, 2254 (1973).

[90] J. A. Odutola and T. R. Dyke, J. Chem. Phys. **72**, 5062 (1980).

[91] J. A. Odutola, T. A. Hu, D. Prinslow, S. E. O'Dell, and T. R. Dyke, J. Chem. Phys. **88**, 5352 (1988).

[92] B.-J. Lee and M. I. Baskes, Phys. Rev. B **62**, 8564 (2000).

[93] R. F. Byrd, P. Lu, J. Nocedal, and C. Zhu, SIAM J. Scient. Stat. Comp. **16**, 1190 (1995).

[94] Ph. Ghosez, J.-P. Michenaud, and X. Gonze, Phys. Rev. B **58**, 6224 (1998).

[95] R. Ludwig, Angew. Chem. Int. Ed. **40**, 1808 (2001).

[96] T. James, D. J. Wales and J. Hernndez-Rojas, Chem. Phys. Lett. **415**, 302 (2005).

[97] D. J. Wales and M. P. Hodges, Chem. Phys. Lett. **286**, 65 (1998).

[98] M. Losada and S. Leutwyler, J. Chem. Phys. **117**, 2003 (2002).

[99] J. Kim and K. S. Kim, J. Chem. Phys. **109**, 5886 (1999).

[100] S. S. Xantheas and T. H. Dunning, J. Chem. Phys. **98**, 8037 (1993).

[101] I. M. B. Nielsen, E. T. Seidel, and C. L. Janssen, J. Chem. Phys. **110**, 9435 (1999).

[102] J. E. Del Bene and J. A. Pople, J. Chem. Phys. **52**, 4858 (1970).

[103] R. Krishnan, J. S. Binkley, R. Seeger, and J. A. Pople, J. Chem. Phys. **72**, 650 (1980).

[104] T. Clark, J. Chandrasekhar, and P. V. R. Schleyer, J. Comput. Chem. **4**, 294 (1983).

[105] N. Pugliano and R. J. Saykally, Science **257**, 1937 (1992).

[106] M. R. Viant, J. D. Cruzan, D. D. Lucas, M. G. Brown, K. Liu, and R. J. Saykally, J. Phys. Chem. A **101**, 9032 (1997).

[107] K. Liu, M. G. Brown, J. D. Cruzan, and R. J. Saykally, Science **271**, 62 (1996).

[108] K. Liu, M. G. Brown, J. D. Cruzan, and R. J. Saykally, J. Phys. Chem. A **101**, 9011 (1997).

[109] K. Liu, M. G. Brown, C. Carter, R. J. Saykally, J. K. Gregory, and D. C. Clary, Nature (London) **381**, 501 (1996).

[110] K. Liu, M. G. Brown, and R. J. Saykally, J. Phys. Chem. A **101**, 8995 (1997).

[111] J. D. Cruzan, L. B. Braly, K. Liu, M. G. Brown, J. G. Loeser and R. J. Saykally, Science **271**, 59 (1996).

[112] J. D. Cruzan, M. R. Viant, M. G. Brown, and R. J. Saykally, J. Phys. Chem. A **101**, 9022 (1997).

[113] The Cambridge Cluster Database, D. J. Wales, J. P. K. Doye, A. Dullweber, M. P. Hodges, F. Y. Naumkin F. Calvo, J. Hernndez-Rojas and T. F. Middleton, http://www-wales.ch.cam.ac.uk/CCD.html.

[114] R. M. Bentwood, A. J. Barnes, W. A. Orville-Thomas, J. Mol. Spect. **84**, 391 (1980).

[115] M. D. Tissandier, S. J. Singer, and J. V. Coe, J. Phys. Chem. A **104**, 752 (2000).

[116] J. B. Paul, C. P. Collier, J. J. Scherer, A. O'Keefe, and R. J. Saykally, J. Chem. Phys. **101**, 5211 (1997).

[117] C. J. Tsai and K. D. Jordan, J. Phys. Chem. **97**, 5208 (1993).

[118] C. J. Tsai and K. D. Jordan, Chem. Phys. Lett. **213**, 181 (1993).

[119] K. Kim, K. D. Jordan, and T. S. Zwier, J. Am. Chem. Soc. **116**, 11568 (1994).

[120] J. M. Pedulla, K. Kim, and K. D. Jordan, Chem. Phys. Lett. **291**, 78 (1998).

[121] E. S. Kryachko, Chem. Phys. Lett. **314**, 353 (1999).

[122] D. M. Upadhyay, M. K. Shukla, and P. C. Mishra, Int. J. Quant. Chem. **81**, 90 (2001).

[123] S. S. Xantheas, C. J. Burnham, and R. Harrison, J. Chem. Phys. **116**, 1493 (2002).

[124] Ch. Janzen, D. Spangenberg, W. Roth, and K. Kleinermanns, J. Chem. Phys. **110**, 9898 (1999).

[125] U. Buck, I. Ettischer, M. Melzer, V. Buch, and V. Sadlej, Phys. Rev. Lett. **80**, 2578 (1998).

[126] R. A. Marcus, Ann. Rev. Phys. Chem. **15**, 155 (1964); A. Warshel, in: *Computer Modeling of Chemical Reactions in Enzymes and Solutions* (Wiley, New York, 1991); Sharon Hammes-Schiffer, Acc. Chem. Res. **34**, 273 (2001).
[127] L. Kemper, K. Muralidharan, Y. Wan, and H.-P. Cheng, *Environment dependent dynamic charge interatomic potential for silica*. Abstract, March Meeting of the American Physical Society, Baltimore, MD (2006).